RASĀYAN *J. Chem.*
Vol. 18 | No. 4 |2179-2186 October-December | 2025
ISSN: 0974-1496 | e-ISSN: 0976-0083 | CODEN: RJCABP
http://www.rasayanjournal.com
http://www.rasayanjournal.co.in

QUANTUM CONFINEMENT AND SURFACE ENGINEERING EFFECTS IN $MAPbBr_3$ NANOPLATELETS AND β-CYCLODEXTRIN-CAPPED QUANTUM DOTS

N. Kumari[1,✉], M. Singh[1], Monika[1] and N. S. Leel[2]
[1]Department of Physics, University of Rajasthan, Jaipur-302004, (Rajasthan) India
[2]Department of Pure and Applied Physics, University of Kota, Kota-324005, (Rajasthan) India
✉Corresponding author: nidhi.meena.2986@gmail.com

ABSTRACT

We report the room-temperature synthesis and comparative characterization of methylammonium (MA) lead bromide ($MAPbBr_3$) nanoplatelets and β-cyclodextrin (β-CD) capped $MAPbBr_3$ quantum dots (QDs). High-resolution transmission electron microscopy (HRTEM) revealed rectangular nanoplatelets (~100 × 50 nm) and spherical QDs with a narrow size distribution (~3.2 ± 0.9 nm). X-ray diffraction (XRD) confirmed the cubic perovskite phase ($Pm\bar{3}m$), with a (100) peak shift from 14.96° (bulk) to 15.48° (nanoplatelets, NPLs), indicating lattice contraction. X-ray photoelectron spectroscopy (XPS) confirmed the presence of Pb^{2+}, Br^-, and $NH3^+$ without signs of oxidation. Optical characterization showed absorption peaks at ~426, ~480, and ~529 nm for nanoplatelets, and blue-shifted peaks (~421, ~455, ~476 nm) for QDs, consistent with quantum confinement. Both morphologies exhibited strong green photoluminescence (PL) at ~523 nm; the QDs displayed narrower emission (FWHM ≈ 24.7 nm) despite their high surface area. This enhanced stability is attributed to β-CD surface passivation, which reduces non-radiative recombination. These findings highlight the morphology-dependent optical and structural behavior of $MAPbBr_3$ nanostructures and the role of β-CD in improving QD stability, making them promising for optoelectronic applications.

Keywords: $MAPbBr_3$, Perovskite Quantum Dots, Nanoplatelets, β-Cyclodextrin, Quantum Confinement, Photoluminescence; Optoelectronics.

RASĀYAN *J. Chem.*, Vol. 18, No.4, 2025

INTRODUCTION

Metal-halide perovskite (MHPs) has emerged as a highly promising material for optoelectronic applications, owing to its outstanding optical tunability and favorable electronic properties.[1-5] These compounds generally adopt the formula ABX_3, where 'A' represents a monovalent cation (Cs^+); 'B' is typically a divalent metal ion like lead (Pb^{2+}); and 'X' denotes a halide anion (Br^-).[6-10] MHPs (NPLs) have been extensively investigated due to their unique properties.[11] $MAPbBr_3$ have garnered immense attention for optoelectronic applications due to their high absorption coefficients, tunable band gaps, and superior PL properties.[12-15] Among their low-dimensional variants, NPLs are of particular interest, offering a distinct intermediate confinement regime between 0D (QDs) and bulk 3D crystals.[11,13,16] Their unique two-dimensional geometry, characterized by atomically thin thickness and extended lateral dimensions, results in anisotropic excitonic behavior, strong quantum confinement in one direction, and enhanced Coulombic interactions.[11,14,17-19] In parallel, surface-passivated QDs, particularly those stabilized with organic macrocycles like β-CD, offer enhanced colloidal stability and reduced surface trap states.[20] β-CD is known to encapsulate MA^+ cations and can provide steric stabilization, prevent aggregation, and improve dispersion in polar environments.[16] Despite widespread use in biomedical and supramolecular fields, β-CD's integration into halide perovskite QD systems for optical applications remains largely unexplored.

Recent efforts have focused on stabilizing $MAPbBr_3$ QDs via encapsulation, nanoporous templating, or doping strategies, but relatively few studies address the specific influence of β-CD on QD growth,

http://doi.org/10.31788/RJC.2025.1849451
This work is licensed under a CC BY 4.0 license.

confinement behavior, or emission control.[8,14,16,20-23] Moreover, very limited reports compare the structural and optical transitions across NPL and QD morphologies within the same $MAPbBr_3$ system under ambient conditions.[14,18,19,24] In this study, we report a room-temperature synthesis and characterization of $MAPbBr_3$ NPLs and β-CD-capped $MAPbBr_3$ quantum dots. HRTEM, XRD, UV–visible absorption, photoluminescence (PL), and XPS are employed to evaluate morphology, crystalline phase, and electronic structure. By comparing structural anisotropy, dimensional confinement effects, and surface chemistry, this work provides a comprehensive understanding of morphology-dependent behavior in $MAPbBr_3$ nanostructures, offering insights for their application in light-emitting and photo-detecting devices.

EXPERIMENTAL

Material and Methods

Methylamine solution (40 wt. % in H_2O), hydrobromic acid (48 wt% in water), lead (II) bromide (98%), oleic acid (OA, technical grade, 90%), oleylamine (OLAm, 70%%), N, N-Dimethylformamide (DMF, 99.8%), ethanol (≥ 99.9 %), toluene (99.8%) and diethyl ether (99.8%), hexylamine and β-Cyclodextrin (β-CD, ≥ 97 %) were purchased from Sigma-Aldrich.

Synthesis of $MAPbBr_3$ Nanoplatelets

The synthesis of $MAPbBr_3$ nanoplatelets was adapted from a previously reported ligand-assisted precipitation method.[19] Briefly, a perovskite precursor solution was prepared by dissolving CH_3NH_3Br and $PbBr_2$ in DMF, with oleic acid and oleylamine as surface ligands. The resulting dispersion was purified by sequential centrifugation, and the nanoplatelets were collected for structural and optical characterization.

Synthesis of β-CD Capped $MAPbBr_3$ Quantum Dots

The synthesis of $MAPbBr_3$/β-CD QDs was adapted from the procedure reported by Huang *et al.* [23] The method involves preparing a perovskite precursor in a polar solvent, followed by the incorporation of β-CD to facilitate a host–guest interaction. Upon antisolvent-induced crystallization, β-CD forms a protective shell around the $MAPbBr_3$ QDs. The resulting β-CD-coated QDs were isolated and dried under vacuum conditions. All reagent ratios and processing parameters were consistent with the original protocol to ensure reproducibility.

Characterization Techniques

The crystalline structure and phase were investigated using X-ray diffraction (XRD) using a PANalytical X'Pert Pro diffractometer (Cu-Kα, λ = 1.5406 Å). HRTEM was performed using a Tecnai G2 20 S-TWIN (FEI, 200 kV) to examine morphology and lattice fringes. Optical absorption spectra were recorded using an Agilent Cary 5000 UV–Vis–NIR spectrophotometer. PL spectra were recorded using a custom-built setup equipped with a 405 nm diode laser. The electronic structure was analyzed by X-ray photoelectron spectroscopy (XPS, Thermo Scientific Nexsa G2).

RESULTS AND DISCUSSION

Morphology and Crystallinity of Nanoplatelets

The morphology and crystallinity of the synthesized $MAPbBr_3$ nanostructures, including both NPLs and β-CD-coated QDs, were investigated by HRTEM. Fig.-1(a) presents an HRTEM image of $MAPbBr_3$ NPLs, exhibiting well-defined 2D morphology with lateral dimensions of approximately 100 nm in length and 50 nm in width. Selected area electron diffraction (SAED) pattern (Fig.-1(b)) shows a combination of spotty ring features and faint radial lines along the diameter, indicating partial crystallinity with semi-oriented domains. Such features are typical for anisotropic structures with some degree of stacking disorder or thickness variation across the NPLs.

A higher magnification image in Fig.-1(c) confirms the presence of well-resolved lattice fringes across the NPL, highlighting their thin crystalline nature. The fringes suggest coherent crystalline domains embedded in an ultrathin matrix. Further zooming into the selected region (Fig.-1(d)) reveals a network of

intersecting lattice fringes oriented in multiple directions, with individual crystalline domains ranging from ~10 nm to ~40 nm.[19] This mosaic-like crystalline texture is consistent with polycrystalline growth confined within 2D nanosheet geometry, supporting earlier XRD observations of preferred (h00) orientation and nanoscale domain sizes.

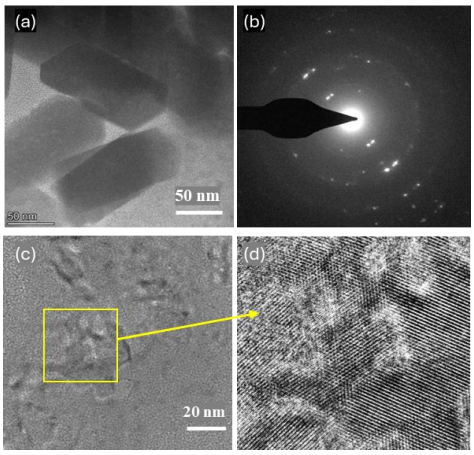

Fig.-1: (a) Low-magnification HRTEM Image of $MAPbBr_3$ NPLs (~100 nm × 50 nm); (b) SAED Pattern Showing Semi-Crystalline Rings; (c) High-Resolution Lattice Fringes; (d) Zoomed Region Showing Polycrystalline Domains (10–40 nm)

Structural Analysis of β-CD Capped Quantum Dots

In contrast, β-CD-capped $MAPbBr_3$ QDs display markedly different morphology. Figure-2(a) shows uniformly dispersed, nearly spherical QDs with sizes below 6 nm. The size histogram (Fig.-2(b)) constructed from multiple particles yields an average diameter of 3.2 ± 0.9 nm, indicating a narrow and controlled size distribution. This confirms the stabilizing effect of the β-CD ligand, which likely passivates surface defects and restricts overgrowth.[23] A wider-field view in Fig.-2(c) illustrates soft agglomeration of QDs, forming low-density clusters with distinguishable particle boundaries. The corresponding SAED pattern (Fig.-2(d)) reveals diffuse rings without distinct spots, indicative of poor crystallinity or amorphous character, likely due to surface passivation and the extremely small core size. Together, these HRTEM results highlight the transition in morphology and crystallinity from well-oriented nanoplates with multiple crystalline domains to ultrasmall QDs stabilized by β-CD, displaying reduced crystallinity. This structural evolution correlates with quantum confinement effects and supports the distinct optical properties (e.g., PL peak at 523 nm) observed in these materials.

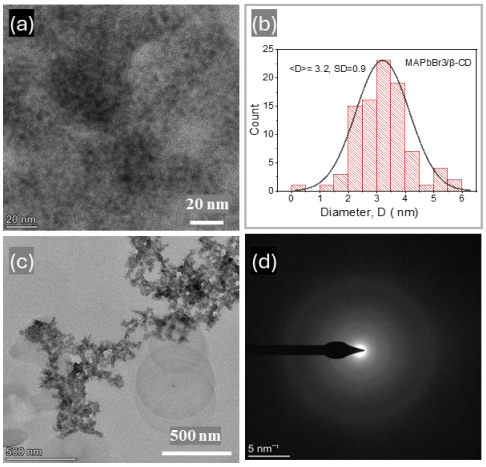

Fig.-2: β-CD Capped $MAPbBr_3$ QDs: (a) HRTEM image of Spherical Particles; (b) Size Histogram (avg. 3.2 ± 0.9 nm); (c) Wide-Field Image; (d) SAED with Diffuse Ring Pattern

X-ray Diffraction Analysis

The structure of the synthesized $MAPbBr_3$ nanoplates was investigated using XRD. The recorded diffraction pattern (Fig.-3) shows well-defined peaks corresponding to the cubic perovskite phase (Pm3m).[19,25] A comparison with the standard bulk $MAPbBr_3$ reference pattern reveals a noticeable shift of the (100) reflection from $2\theta \approx 14.96°$ (bulk) to 15.48° in the nanoplates, indicating a slight lattice contraction. This shift is attributed to compressive strain induced by thickness confinement in the 2D morphology [25] . The diffraction peaks were indexed based on the cubic symmetry as follows: (100) at 15.48° (d = 5.72 Å), (110) at 21.74° (d = 4.09 Å), (200) at 30.70° (d = 2.91 Å), (210) at 34.34° (d = 2.61 Å), (211) at 38.10° (d = 2.36 Å), (220) at 43.72° (d = 2.07 Å), (300) at 46.50° (d = 1.95 Å), (310) at 51.36° (d = 1.78 Å), (321) at 63.32° (d = 1.47 Å), and (400) at 65.40° (d = 1.43 Å). The dominance of the (100) and (200) reflections, with an intensity ratio $I(200)/I(100) \approx$ of 0.70, alongside the significant suppression of non-(h00) peaks, confirms strong preferred orientation along the (h00) planes. This orientation is typical of 2D NPL structures where the crystal grows laterally and is confined in thickness. Crystallite sizes were estimated using the Scherrer equation .[25] The (100) and (200) reflections yielded average crystallite sizes of ~54.2 nm and ~42.8 nm, respectively. Other peaks showed crystallite sizes ranging from ~20 to 102 nm. These values are consistent with the limited grain growth expected in nanostructures and support the presence of highly crystalline yet dimensionally confined domains. The structural findings from XRD correlate well with the observed morphology in high-resolution transmission electron microscopy, where stacked nanosheets with well-aligned lattice fringes were identified. The crystallographic orientation and domain sizes observed are also in agreement with the optoelectronic behavior of the material, particularly the strong PL emission observed at 523 nm, characteristic of green-emitting $MAPbBr_3$ nanostructures.

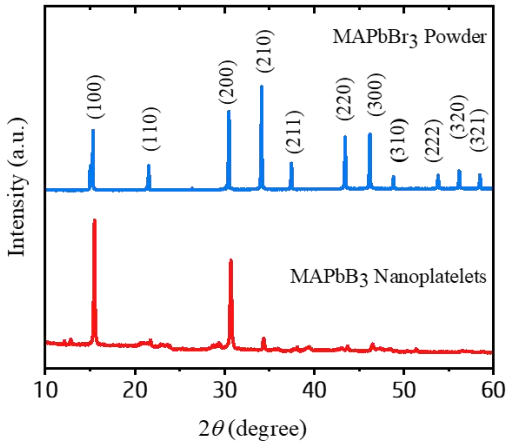

Fig.-3: XRD Pattern of $MAPbBr_3$ NPLs Compared with Bulk Reference

XPS Analysis

High-resolution XPS spectra were recorded for the C 1s, N 1s, Br 3d, and Pb 4f core levels as depicted in Fig.-4 (a) to (d). All spectra were fitted using Voigt line shapes.[26] The baseline was modelled using a Shirley-type background. The binding energy (BE) scale was calibrated using the adventitious carbon C 1s peak, which was set to 284.8 eV, serving as an internal reference.[26] This calibration ensured accurate assignment of all other elemental core levels. The C 1s spectrum (Fig.-4(a)) shows a dominant peak at 284.8 eV, assigned to C–C/C–H, and a secondary component near 285.78 eV, which can be attributed to NH_3^+ within the MA^+ cation.[26,27] Additional contributions in the range of 285.3–288.5 eV reported in previous studies are often related to environmental exposure or decomposition species like CH_3 NH_2 and CH_3I.[27] The N 1s spectrum (Fig.-4(b)) displayed a strong signal at 401.96 ± 0.006 eV, corresponding to the NH_3^+ group in MA^+, in line with typical reported BE values between 400.8–402.5 eV.[27,28] A minor component at 400.01 ± 0.066 eV, which may indicate surface decomposition or adsorbed nitrogen-

containing species.[27] Br 3d spectrum (Fig.-4(c)) is resolved into two components, Br $3d_{5/2}$ and Br $3d_{3/2}$, located at 68.42 eV and 69.44 eV, respectively, with a spin–orbit splitting of ~1.02 eV. [29,30] These values agree with standard reference values for halide perovskites, where Br $3d_{5/2}$ typically appears at 68.5 ± 0.2 eV. [27,29] The Pb 4f spectrum (Fig.-4(d)) is characterized by two strong peaks at 138.34 eV (Pb $4f_{7/2}$) and 143.20 eV (Pb $4f_{5/2}$), with a splitting of ~4.86 eV. [27,29,31] These values are slightly lower than those reported for $MAPbBr_3$ in some cases (~139.1 eV), which may be due to the influence of the halide environment and possible surface effects.[27,31] The observed core-level positions and their relative intensities confirm the Pb^{2+} oxidation. These XPS results confirm the expected stoichiometry and chemical environment of $MAPbBr_3$, validating the successful incorporation of MA^+, lead, and bromide into the perovskite structure.

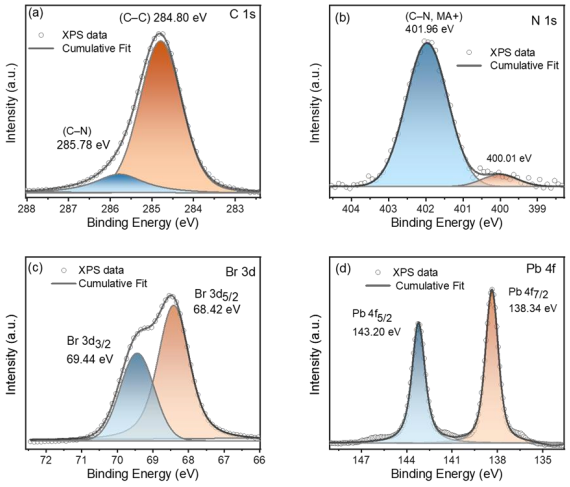

Fig.-4: High-resolution XPS Spectra of $MAPbBr_3$: (a) C 1s Core Level, (b) N 1s Peak from MA+, (c) Br 3d Doublet with Splitting of ~1.02 eV, (d) Pb 4f Doublet with Splitting of ~4.86 eV. All Spectra Were Fitted using Voigt Line Shapes to Account for both Instrumental (Gaussian) and Lifetime (Lorentzian) Broadening Effects

Optical Properties

The optical properties of MAPbBr nanostructures were investigated using UV–Vis absorption and PL spectroscopy(Fig.-5).

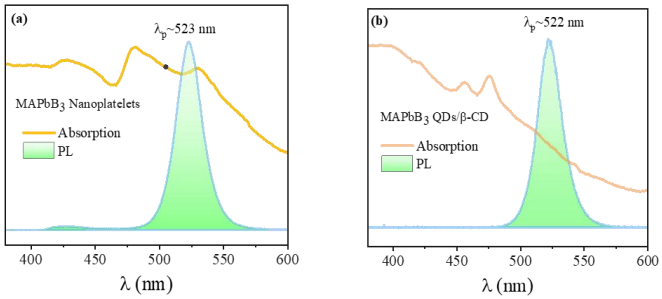

Fig.-5: (a) UV–Vis and PL Spectra of $MAPbBr_3$ NPLs Showing Absorption Peaks at ~426, ~480, and ~529 nm and Green Emission at 523.4 nm. (b) Spectra of β-CD Capped $MAPbBr_3$ QDs with Blue-Shifted Absorption (~421, ~455, ~476 nm) and Emission at 523.2 nm

For NPLs (Fig.-5 (a)), the UV–Vis spectrum shows distinct absorption peaks at ~426, ~480, and ~529 nm, attributed to excitonic transitions and band-edge absorption in 2D-confined structures .[11,25,32] The PL spectrum, recorded under 405 nm diode laser excitation, exhibits a strong green emission at 523.4 ± 0.02 nm with a full-width at half maximum (FWHM) of ~25.9 ± 0.35 nm, fitted using a Voigt model (Gaussian: ~17.8 nm, Lorentzian: ~11.3 nm).[25,33] The narrow linewidth and symmetric profile indicate

high structural uniformity, consistent with the crystalline domains observed in HRTEM and XRD. For β-CD capped QDs (Fig.-5 (b)), the UV–Vis spectrum reveals blue-shifted absorption peaks at ~421, ~455, and ~476 nm, reflecting stronger quantum confinement due to the smaller particle size.[14,23,34] The PL emission is centered at 523.2 ± 0.03 nm with a slightly narrower FWHM of ~24.7 ± 0.38 nm (Gaussian: ~17.9 nm, Lorentzian: ~9.1 nm), on confinement, and reduced size dispersion due to β-CD passivation.[14,23] The strong and stable PL emission at ~523 nm indicates effective surface passivation by β-cyclodextrin. This suggests reduced surface trap density and enhanced optical stability under ambient conditions. The optical data confirm morphology-dependent electronic properties, with QDs exhibiting tighter confinement compared to NPLs.

CONCLUSION

In this study, $MAPbBr_3$ nanoplatelets and β-cyclodextrin (β-CD) capped $MAPbBr_3$ quantum dots were synthesized at room temperature and systematically characterized. HRTEM and XRD confirmed the morphology and crystallinity of both nanostructures, with nanoplatelets exhibiting preferred orientation and lattice contraction. XPS analysis verified the expected chemical states (Pb^{2+}, Br^-, MA^+) and absence of surface oxidation. Optical measurements revealed size- and morphology-dependent behavior, with quantum dots exhibiting blue-shifted absorption and narrower PL emission due to stronger confinement. Despite their small size and high surface area, β-CD-capped QDs demonstrated strong and stable photoluminescence, indicating effective surface passivation. These results emphasize the role of dimensional control and organic passivation in tailoring the optical and structural properties of perovskite nanomaterials, offering a viable route for developing stable and efficient perovskite-based optoelectronic devices.

ACKNOWLEDGMENTS

The authors gratefully acknowledge the Head of the Department of Physics, University of Rajasthan, for providing access to the XPS and UV–vis spectroscopy facilities. The authors also acknowledge the financial support from the Science and Engineering Research Board (SERB), Department of Science and Technology, Government of India (Project No: PDF/2018/003146).

CONFLICT OF INTERESTS

The authors declare that there is no conflict of interest.

AUTHOR CONTRIBUTIONS

The present work is related to *SDG-7: Affordable and Clean Energy*. All the authors contributed significantly to this manuscript, participated in reviewing/editing and approved the final draft for publication. The research profile of the authors can be verified from their ORCID ids, given below:

N. Kumari https://orcid.org/0009-0003-0749-8040
M. Singh https://orcid.org/0000-0002-9519-0307
Monika https://orcid.org/0009-0008-9227-4792
N.S. Leel https://orcid.org/0009-0006-5017-270X

Open Access: This article is distributed under the terms of the Creative Commons Attribution 4.0 International License (http://creativecommons.org/licenses/by/4.0/), which permits unrestricted use, distribution, and reproduction in any medium, provided you give appropriate credit to the original author(s) and the source, provide a link to the Creative Commons license, and indicate if changes were made.

REFERENCES

1. A. Kojima, K. Teshima, Y. Shirai, T. Miyasaka, *Journal of the American Chemical Society*, **131**, 6050(2009), https://doi.org/10.1021/ja809598r
2. J. Burschka, N. Pellet, S.-J. Moon, R. Humphry-Baker, P. Gao, M. K. Nazeeruddin, M. Grätzel, *Nature*, **499**, 316(2013), https://doi.org/10.1038/nature12340
3. S. D. Stranks, G. E. Eperon, G. Grancini, C. Menelaou, M. J. P. Alcocer, T. Leijtens, L. M. Herz, A. Petrozza, H. J. Snaith, *Science*, **342**, 341(2013), https://doi.org/10.1126/science.1243982

4. Y. Shang, G. Li, L. Liu, F. Meng, Z. Li, *Science Advances*, **5**, eaaw8072(2019), https://doi.org/10.1126/sciadv.aaw8072
5. L. N. Quan, F. P. García de Arquer, R. P. Sabatini, E. H. Sargent, *Advanced Materials*, **30**, 1801996(2018), https://doi.org/10.1002/adma.201801996
6. C. C. Stoumpos, M. G. Kanatzidis, *Accounts of Chemical Research*, **48**, 2791(2015), https://doi.org/10.1021/acs.accounts.5b00229
7. F. Ruf, M. F. Aygüler, N. Giesbrecht, B. Rendenbach, P. Docampo, T. Bein, *APL Materials*, **7**, 031113(2019), https://doi.org/10.1063/1.5083792
8. D. Rambabu, S. Bhattacharyya, T. Singh, C. M. L., T. K. Maji, *Inorganic Chemistry*, **59**, 1436(2020), https://doi.org/10.1021/acs.inorgchem.9b03183
9. J. Endres, M. Kulbak, L. Zhao, B. P. Rand, D. Cahen, G. Hodes, A. Kahn, *The Journal of Physical Chemistry Letters*, **7**, 2722(2016), https://doi.org/10.1021/acs.jpclett.6b00946
10. L. N. Quan, F. P. García de Arquer, R. P. Sabatini, E. H. Sargent, *Advanced Materials*, **30**, 1801996(2018), https://doi.org/10.1002/adma.201801996
11. C. Otero-Martínez, M. García-Batlle, J. Ye, M. Sessolo, H. J. Bolink, *Advanced Materials*, **34**, 2107105(2022), https://doi.org/10.1002/adma.202107105
12. X. Zhang, L. Xu, Y. Li, S. SaeidNahaei, *Solid State Communications*, **356**, 114965(2022), https://doi.org/10.1016/j.ssc.2022.114965
13. J.-Y. Zheng, Y.-F. Wang, Y.-H. Tian, H.-B. Yang, Y.-H. Jiang, Z.-K. Wang, *Scientific Reports*, **9,** 11738(2019), https://doi.org/10.1038/s41598-019-47902-1
14. N. Droseros, G. Longo, J. C. Brauer, M. Sessolo, H. J. Bolink, N. Banerji, *ACS Energy Letters*, 3, 1458(2018), https://doi.org/10.1021/acsenergylett.8b00475
15. L.-C. Chen, K.-L. Lee, C.-Y. Huang, J.-C. Lin, Z.-L. Tseng, *Micromachines*, **9**, 205(2018), https://doi.org/10.3390/mi9050205
16. F. Zhang, H. Zhong, C. Chen, X.-G. Wu, X. Hu, H. Huang, J. Han, B. Zou, Y. Dong, *ChemNanoMat*, **3,** 303(2017), https://doi.org/10.1002/cnma.201700034
17. X. Bai, H. Zhang, Q. Cao, J. Wang, W. Zhang, Y. Fu, *Advanced Optical Materials*, **12**, 2400221, (2024), https://doi.org/10.1002/adom.202400221
18. M. Richter, *Physical Review Materials*, **1**, 016001(2017), https://doi.org/10.1103/PhysRevMaterials.1.016001
19. S. Huang, G. Zhang, Y. Zhang, H. Zhang, *Journal of Luminescence*, **220**, 116984(2020), https://doi.org/10.1016/j.jlumin.2019.116984
20. Q.-L. Li, W.-X. Lu, N. Wan, S.-N. Ding, *Chemical Communications*, **52**, 12342(2016), https://doi.org/10.1039/C6CC04908G
21. H. Cheng, Y. Zhang, Z. Zhang, Y. Wu, J. Yang, X. Wang, *The Journal of Physical Chemistry Letters*, **15**, 4792(2024), https://doi.org/10.1021/acs.jpclett.4c00862
22. J. Bartolomé, M. Vila, C. Redondo-Obispo, A. de Andrés, C. Coya, *Nanomaterials*, **13**, 2513, (2023), https://doi.org/10.3390/nano13182513
23. S. Huang, G. Zhang, Y. Zhang, H. Zhang, *ChemNanoMat*, **5**, 1311(2019), https://doi.org/10.1002/cnma.201900381
24. B. Liu, Y. Han, Y. Li, X. Wang, H. Zhang, *Optics Express*, **28**, 10714(2020), https://doi.org/10.1364/OE.378203
25. A. Niebur, E. Klein, R. Lesyuk, C. Klinke, J. Lauth, *Advanced Optical Materials*, **13**, 2402923(2025), https://doi.org/10.1002/adom.202402923
26. G. Greczynski, L. Hultman, *Journal of Applied Physics*, **132**, 011101(2022), https://doi.org/10.1063/5.0086359
27. S. Béchu, M. Ralaiarisoa, A. Etcheberry, P. Schulz, *Advanced Energy Materials*, **10,** 1904007(2020), https://doi.org/10.1002/aenm.201904007
28. K. Zhang, M. Zhang, N. Zhu, H. Yin, J. Xing, L. Wang, *Journal of Materials Science*, **56**, 11436(2021), https://doi.org/10.1007/s10853-021-06022-w

29. R. Lindblad, N. K. Jena, B. Philippe, J. Oscarsson, D. Bi, E. M. J. Johansson, M. Odelius, H. Johansson, M. T. Borgström, H. Rensmo, *The Journal of Physical Chemistry C*, **119**, 1818(2015), https://doi.org/10.1021/jp509460h
30. E. Choi, H. Lee, Y. Kim, J. Lee, D. Kim, *npj 2D Materials and Applications*, **6**, 44(2022), https://doi.org/10.1038/s41699-022-00317-5
31. M. Liu, J. Pan, L. Zhao, B. Li, Y. Zhang, B. Dong, *Advanced Science*, **4**, 1700335(2017), https://doi.org/10.1002/advs.201700335
32. A. Naeem, F. Masia, S. Christodoulou, I. Moreels, P. Borri, W. Langbein, *Physical Review B*, **91**, 121302(2015), https://doi.org/10.1103/PhysRevB.91.121302
33. J. Q. Grim, S. Christodoulou, F. Di Stasio, R. Krahne, R. Cingolani, L. Manna, *Nature Nanotechnology*, **9**, 891, (2014), https://doi.org/10.1038/nnano.2014.213
34. J. Sun, M. Chen, T. Huang, G. Ding, Z. Wang, *Nanomaterials*, **14**, 1546(2024), https://doi.org/10.3390/nano14191546

[RJC-9451/2025]